

# A study of the metal-rich, thick disk globular cluster NGC 5927 <sup>★</sup>

## A stellar inventory

J. Simmerer<sup>1,2</sup>, S. Feltzing<sup>1</sup>, and F. Primas<sup>3</sup>

<sup>1</sup> Lund Observatory, Box 43, SE-221 00 Lund, Sweden  
e-mail: sofia@astro.lu.se

<sup>2</sup> University of Utah Department of Physics and Astronomy, Salt Lake City, UT 84112  
e-mail: jennifer@physics.utah.edu

<sup>3</sup> European Southern Observatory, Karl-Schwarzschild Str. 2, 85748 Garching b. München, Germany  
e-mail: fprimas@eso.org

Received 2012-11-14; accepted 2013-04-23

### ABSTRACT

We present a list of 72 radial velocity member stars in the metal-rich globular cluster NGC 5927. The radial velocities are based on multi-epoch, multi-fibre spectra. We identify 46 RGB/HB stars and 26 turn-off stars that are radial velocity members in the cluster. This cluster is situated quite close to the disk and hence fore- and/or background contamination, especially in the outskirts of the cluster, can be quite severe. Fortunately, the cluster has a radial velocity (we determine it to  $v_r = -104.03 \pm 5.03 \text{ km s}^{-1}$ ) that sets it clearly apart from the bulk velocities of the surrounding, background, and foreground stellar populations. Hence, our identification of members is clean and we can quantify a 50% contamination when stars in the outer part of the cluster are selected solely based on position in the colour-magnitude diagram as opposed to selections based on radial velocities.

**Key words.** Globular clusters: individual: NGC 5927, Stars: kinematics and dynamics

## 1. Introduction

It has long been recognized that the globular cluster system in the Milky Way contains at least two distinct groups: a metal-poor system and a metal-rich system (Zinn 1985). While some individual clusters might be accreted from satellite systems, metal-poor clusters are typically associated with the halo (Bica et al. 2006; Law & Majewski 2010). The metal-rich subsystem is strongly concentrated around and therefore typically associated with the Galactic bulge (Bica et al. 2006). Additional structure in the metal rich-system was originally proposed by Armandroff (1989), who suggested that these clusters were kinematically associated with the stellar thick disk. Proper motion studies confirm Bulge membership for some metal-rich clusters for which orbits can be derived (Dinescu et al. 1999a,b, 2003; Casetti-Dinescu et al. 2007, 2010). However, a few clusters may still be associated with the thick disk. One of the best thick disk candidate clusters is NGC 5927 (Casetti-Dinescu et al. 2007).

No detailed spectroscopic abundance analysis of NGC 5927 has been published in the last 20 years despite evidence that the overall metallicity of the cluster is poorly constrained. Based on Ca II IR triplet measurements by Rutledge et al. (1997a), three different calibrations yield varying results:  $-0.34$  dex (Zinn-scale),  $-0.64$  dex (Carretta & Gratton -scale), and  $-0.67$  dex (Kraft & Ivans 2003). Thomas et al. (2003) used Lick indices to derive  $[\text{Fe}/\text{H}] = -0.21 \pm 0.11$ .

At  $l \simeq 34^\circ$  contamination from the background (Bulge) population is of small concern and the foreground contamination is expected to be moderate (but as we shall see it is still signif-

icant). This property has made NGC 5927 a popular empirical fiducial cluster in studies of extra-galactic resolved stellar populations and it is often used as a template for colour-magnitude diagrams, integrated colours, and spectra of metal-rich, single age stellar populations. Recent examples include Brown et al. (2004, 2005) Bedin et al. (2005), and Santos & Piatti (2004).

For these reasons it is interesting to provide a clean sample of members of the cluster that can be used for further detailed studies, e.g., as targets for high-resolution spectroscopic studies. In this paper we present a VLT-FLAMES observation of a large number of stars in this cluster and derive the radial velocities of the stars as well as the systemic velocity of the cluster.

## 2. Selection of targets

The selection of targets in NGC 5927 was done for three different types of stars: horizontal branch (HB) stars, red giant branch (RGB) stars, and turn-off (TO) stars. Seven bright HB and RGB stars were observed at high resolution ( $R \sim 40\,000$ ) and will be referred to as HB/RGB-UVES. The remaining RGB targets were observed at lower resolution ( $R \sim 20\,000$ ) and will be referred to as RGB-GIRAFFE. Target selection was based on photometric color cuts and designed to maximize the number of fibres allocated to stars.

HB and RGB stars for high resolution fibres (HB/RGB-UVES) were selected using a colour-magnitude diagram (CMD) based on observations with the Advanced Camera for Surveys (ACS) on-board Hubble. The selection of HB/RGB-UVES stars was straightforward. The ACS CMD allowed us to select targets in

<sup>★</sup> Based on observations collected at the European Southern Observatory, Chile, ESO, Programme ID 079.B-0721(A)

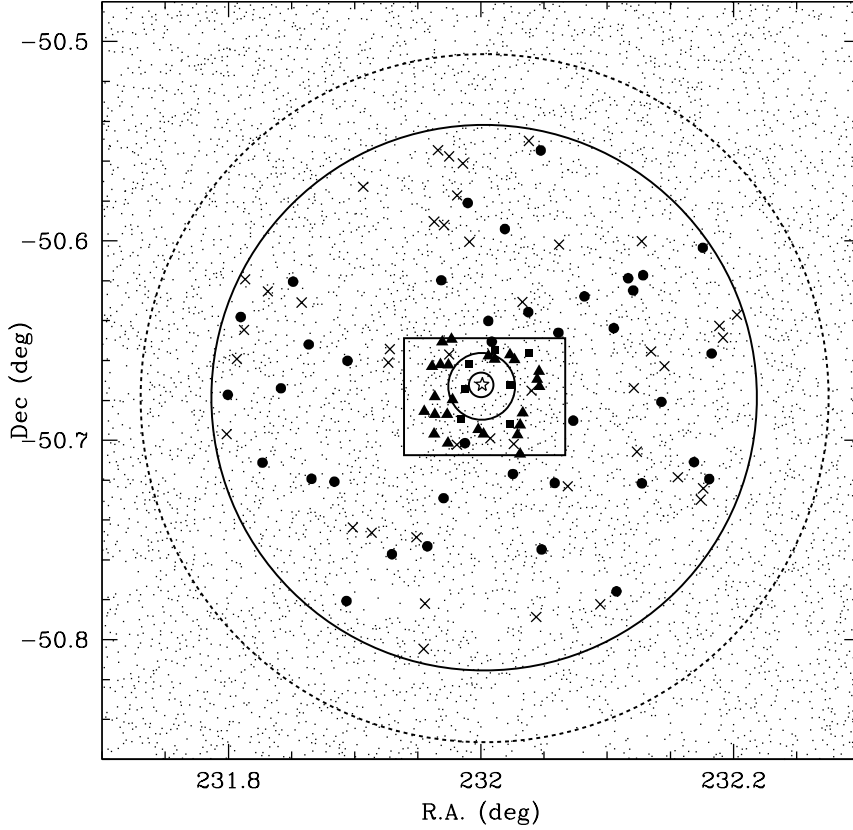


**Fig. 1.** Position on the sky of all the fibres. Filled squares mark HB/RGB-UVES stars with radial velocity membership. RGB-GIRAFFE stars and TO radial velocity members are marked with filled circles and filled triangles, respectively. Crosses mark all stars that are non-members according to their radial velocities. The core and half-mass radii are marked as circles close to the centre of the cluster (which is marked by an open star). The tidal radius is also marked with a circle with a dashed line. Data for the various radii were taken from the latest web-based version of Harris (1996). The FLAMES field of view is indicated by a large solid circle. The square shows the rough position of the ACS camera observations.

**Table 1.** Basic data for candidate HB and RGB stars observed with UVES ( $R \sim 40\,000$ ) in NGC 5927.

Star	2MASS ID	R.A. (fibre)	Dec. (fibre)	$v_{\text{Helio}}$ [km s $^{-1}$ ]	$\sigma$ [km s $^{-1}$ ]	$V_{606}$	$I_{814}$	$J$	$H$	$K_S$
NGC 5927-01	15275603-5041223	15 27 56.16	-50 41 22.20	-102.01	0.37	16.02	15.83	13.355	12.619	12.565
NGC 5927-02		15 27 56.88	-50 40 28.20	-94.39	0.19	16.12	15.94			
NGC 5927-03	15275764-5039423	15 27 57.60	-50 39 42.12	-101.05	0.36	16.16	15.98	13.707	13.021	12.891
NGC 5927-04	15280273-5039163	15 28 02.64	-50 39 16.20	-105.61	0.52	16.03	15.88		12.282	12.129
NGC 5927-05	15280546-5040214	15 28 05.52	-50 40 21.72	-105.37	0.46	16.04	15.82	13.026	12.432	12.161
NGC 5927-06	15280537-5041317	15 28 05.28	-50 41 31.56	-102.34	0.44	16.19	16.09	13.738	13.012	12.917
NGC 5927-07		15 28 09.12	-50 39 22.32	-105.84	0.56	16.08	15.88			

Column one the IDs used by us for the stars while column two gives the 2MASS identification. Columns three and four contain the target fibre coordinates, column five the heliocentric radial velocity, and column six the radial velocity standard deviation as derived in Sect. 4. Columns seven and eight list the in-flight ACS magnitudes (T. Brown *priv. com.*). The last three columns list the  $JHK_S$  magnitudes from 2MASS.

the crowded core of the cluster, increasing our chances of observing cluster members (compare Fig. 2).<sup>1</sup>

<sup>1</sup> At the time of selection this photometry was unpublished. Later a refereed publication of this data was published in (Brown et al. 2005). T. Brown has kindly provided us with both the calibrated ACS photom-

The final list of HB/RGB-UVES targets is given in Table 1. These targets are bright enough to have 2MASS NIR photometry (Skrutskie et al. 2006).  $JHK_S$  magnitudes are included in the table if their respective quality flag is at least “B”. NGC 5927-02

etry and his astrometric solution. Our target cross-match was done in RA and Dec. We found target matches for every star on the HB/RGB

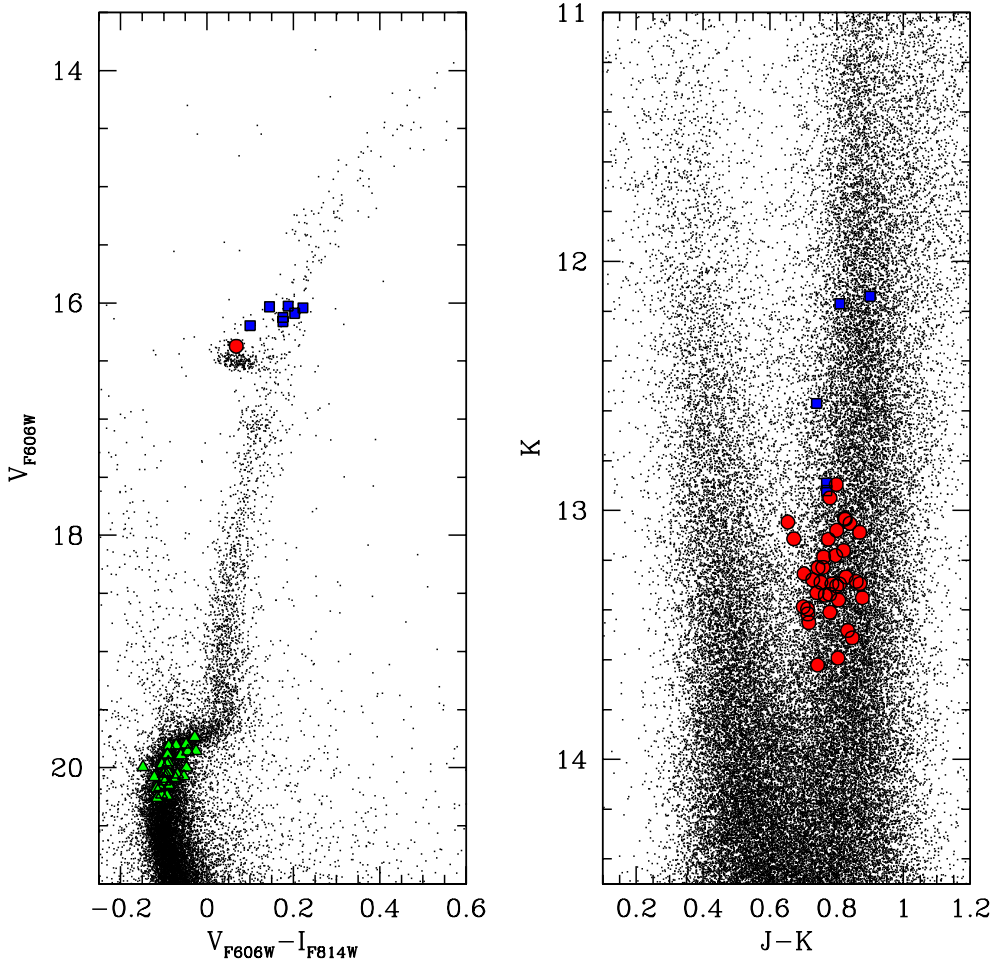


**Fig. 2.** Position of program stars in color-magnitude diagrams. **Left:** RGB-UVES (light blue squares), RGB-GIRAFFE (red circles), and TO stars (green triangles) from HST ACS photometry. **Right:** RGB-UVES and RGB-GIRAFFE stars from 2MASS photometry. Black dots indicate the full CMDs.

and -07 have no reliable 2MASS photometry and NGC 5927-05 and NGC 5927-06 have contamination flagged for its  $JHK_S$  magnitudes.

TO stars were selected from the same ACS CMD as the HB/RGB-UVES stars. A small box was placed around the TO in the CMD. In total 30 suitable TO star were selected. These are listed in Table 2 and their positions in the CMD are shown in Fig. 1.<sup>2</sup>

RGB stars for low-resolution fibres (RGB-GIRAFFE) were selected from a CMD based on 2MASS photometry (Skrutskie et al. 2006). These targets were selected to be further from the core of the cluster in order facilitate the positioning of the fibres, but also to probe the cluster properties to larger radii. The stars were selected to roughly match the magnitudes of the HB/RGB-UVES stars with  $13.6 < K_S < 12.8$  (compare CMD in Fig. 2). In total 75 RGB-GIRAFFE candidate stars were selected and observed. They are listed in Table 3 along with the associated fibre coordinate, the 2MASS identification, and the  $JHK_S$  magnitudes.

<sup>2</sup> We also cross-matched these stars with the final photometry and astrometry from T. Brown and found that all stars apart from T051 have a unique match.

The position of all targets on the sky is shown in Fig. 1. Since our targets are drawn from two different photometric sources, our fibre coordinate system represents a compromise between two astrometric systems. For the sake of presenting a single internally consistent coordinate system and aiding future cross-identification, we list the R.A. and Dec. for the fibre positions in Tables 1, 2, and 3 rather than the astrometry used in the selection. Fibre coordinates are within  $0.5''$  of the ACS coordinates (Brown et al. 2005) and within  $0.13''$  (RGB-GIRAFFE targets) or  $1.0''$  (HB/RGB-UVES targets) of the 2MASS coordinates.

### 3. Observations and data reduction

For the seven high-resolution ( $R \sim 40,000$ ) fibres allocated to HB/RGB-UVES targets we used the setting centered at 580 nm which covers the spectrum between 480.0 nm and 682.0 nm with a gap between 577.5 and 582.5 nm (CCD#3, filter SHP700, red arm only). For the 105 ( $R \sim 20,000$ ) Medusa fibres, we selected the grating setting HR13. HR13 (612.0 – 640.5 nm) includes several astrophysically interesting elements (e.g. O, Na, and Ba) and still provides adequate throughput for the fainter TO stars.

Due to the crowding in the central part of the cluster, good seeing was imperative and therefore the observations were carried out in service mode using the FLAMES spectrograph (Pasquini et al. 2002) mounted on UT2 on Paranal. The seeing requirement was set to  $1.2''$  for the service mode observations to

**Table 2.** Basic data for candidate TO stars observed with GIRAFFE in NGC 5927.

Star	R.A. (fibre)	Dec. (fibre)	R.V. [km s <sup>-1</sup> ]	$V_{606}$	$(V_{606} - I_{814})$
TO001	15 27 49.25	-50 41 08.00	-103.74	20.11	-0.097
TO004	15 27 50.70	-50 39 46.40	-107.32	20.23	-0.105
TO012	15 27 51.21	-50 40 41.10	-106.90	19.81	-0.088
TO013	15 27 52.64	-50 39 02.20	-98.06	20.05	-0.101
TO014	15 27 51.24	-50 41 13.50	-99.88	20.24	-0.092
TO015	15 27 52.31	-50 39 43.10	-96.88	19.80	-0.048
TO016	15 27 51.12	-50 41 48.70	-118.28	20.16	-0.109
TO021	15 27 53.81	-50 39 44.20	-111.05	19.97	-0.104
TO022	15 27 54.42	-50 38 57.60	-102.84	19.89	-0.060
TO033	15 27 53.58	-50 41 13.30	-110.28	20.04	-0.097
TO036	15 27 54.61	-50 40 46.50	-105.18	19.99	-0.148
TO037	15 27 53.72	-50 42 05.10	-99.15	19.85	-0.025
TO051 †	15 27 59.47	-50 41 40.70	-105.33		
TO052	15 28 1.45	-50 39 27.30	-102.29	20.04	-0.090
TO054	15 28 0.52	-50 41 49.00	-105.52	20.05	-0.068
TO056	15 28 2.62	-50 39 33.50	-110.10	20.09	-0.101
TO064	15 28 5.51	-50 39 25.70	-99.61	19.88	-0.091
TO070	15 28 6.40	-50 39 34.60	-104.23	20.00	-0.047
TO083	15 28 6.97	-50 41 50.20	-106.09	20.15	-0.088
TO084	15 28 7.43	-50 41 32.50	-105.61	20.07	-0.053
TO086	15 28 7.93	-50 41 10.50	-103.21	19.97	-0.092
TO088	15 28 7.43	-50 42 24.90	-93.08	20.14	-0.085
TO090	15 28 9.62	-50 40 30.50	-103.40	20.26	-0.115
TO101	15 28 10.67	-50 40 10.00	-107.09	19.80	-0.071
TO103	15 28 11.03	-50 39 55.70	-108.89	20.08	-0.122
TO106	15 28 11.14	-50 40 22.60	-95.77	19.95	-0.089
TO020	15 27 53.96	-50 39 24.90	13.82	19.74	-0.028
TO042	15 27 55.43	-50 42 8.20	15.37	20.09	-0.073
TO058	15 28 1.78	-50 41 56.60	9.71	19.86	-0.044
TO078	15 28 6.25	-50 42 6.80	32.98	20.18	-0.117

Fibre coordinates are given in columns two and three. Column four contains the heliocentric radial velocity derived from the combined spectrum (see Sect. 4). The last columns contain the in-flight ACS magnitudes (T. Brown *priv. com.*). The first 26 lines contain the stars with a radial velocity that makes them likely members of NGC 5927. The last four entries are the stars that fall more than  $3\sigma$  outside the mean cluster radial velocity.

† Star T051 has no detection in the Brown photometry within 1.5 arcsec. There are two sources within 1.7 arcseconds. We cannot unambiguously associate colors from Brown et al. (2005) with our target source.

minimize the loss of light due to finite fibre size and at the same time maximize the amount of useful observing time available. The explicit aim was, for each observing block (OB), to achieve  $S/N=11$  @630nm for HB/RGB-UVES stars,  $S/N=4$  @620nm for TO stars, and  $S/N=25$  for HB-GIRAFFE stars. Each OB was observed for 3600 s. In total we observed 20 OBs. Observations were carried out in service mode during May and July 2007. The observing conditions for each OB are listed in Table 4. The estimated  $S/N$  were achieved.

Initially, the data were reduced as part of the ESO service mode operations using the GIRAFFE pipeline version 1.0<sup>3</sup>. Upon inspection it soon became clear that what is known as the “CCD glow” was a serious problem for our spectra. This glow shows itself in the form of a higher background in one corner of the CCD. In particular it affects fibres with higher numbers. It was thus necessary to undertake a re-reduction of the data. This was done using the  $\beta$ -version of the GIRAFFE pipeline version 2.3, released specifically to deal with the CCD glow.

Before combining the spectra from the 20 OBs into a final spectrum with increased  $S/N$  the necessary helio-centric cor-

rections, as calculated within IRAF<sup>4</sup> were applied (see Table 4). For a few RGB-GIRAFFE stars some spectra were rejected (see Table 5 and the discussion in Sect. 4.1). In some cases there were also one out of the 20 spectra that was not usable (e.g., due to a slight off-set in the placement of the fibre, resulting in a too low flux). The spectra were combined using the `SCOMBINE` task in IRAF, using a min-max rejection. A few example spectra are shown in Figure 3.

#### 4. Determination of radial velocities

Radial velocities were derived using the task `FXCOR` in IRAF. The task cross-correlates a template spectrum with the target spectrum and reports the velocity difference between the two. Given the wide range of stellar evolutionary states in the data set, no single template would adequately serve for all the stars. Both the RGB-UVES and RGB-GIRAFFE spectra were matched to the observed high-resolution spectrum of NGC 5927-01 shifted onto a rest wavelength scale. We attempted the same procedure for the TO stars, but the very low  $S/N$  in these spectra and the intrinsically greater template spectrum mismatch made this impractical.

<sup>3</sup> See <http://www.eso.org/sci/software/pipelines/> for a listing of the GIRAFFE pipeline versions.

<sup>4</sup> IRAF is distributed by National Optical Astronomy Observatories, operated by the Association of Universities for Research in Astronomy, Inc., under contract with the National Science Foundation, USA.

**Table 3.** Basic data for candidate RGB stars observed with GIRAFFE in NGC 5927.

Star	2MASS ID	Cluster members						Star	2MASS ID	Cluster non-members					
		R.A.	Dec	$J$	$H$	$K_S$	R.A.			Dec	$J$	$H$	$K_S$		
M003	15280206-5039020	15 28 2.06	-50 39 2.00	14.08	13.39	13.3	M130	15274240-5039396	15 27 42.40	-50 39 39.60	14.21	13.61	13.38		
M012	15275697-5042051	15 27 56.97	-50 42 5.10	13.88	13.17	13.08	M138	15274271-5039153	15 27 42.71	-50 39 15.30	13.81	13.06	12.98		
M061	15280140-5038244	15 28 1.40	-50 38 24.40	14.1	13.43	13.27	M171	15281652-5043230	15 28 16.52	-50 43 23.00	14.25	13.52	13.38		
M098	15280608-5043008	15 28 6.08	-50 43 0.80	14.17	13.56	13.36	M211	15282906-5040257	15 28 29.06	-50 40 25.70	13.99	13.31	13.16		
M111	15280900-5038085	15 28 9.00	-50 38 8.50	14.36	13.6	13.51	M213	15275781-5036016	15 27 57.81	-50 36 1.60	13.6	12.86	12.72		
M115	15281754-5041246	15 28 17.54	-50 41 24.60	14.23	13.53	13.35	M222	15274775-5044550	15 27 47.74	-50 44 55.00	14.4	13.7	13.53		
M120	15281471-5038457	15 28 14.71	-50 38 45.70	13.95	13.27	13.19	M227	15282965-5042205	15 28 29.65	-50 42 20.50	14.06	13.48	13.24		
M126	15280789-5037501	15 28 7.89	-50 37 50.10	13.97	13.33	13.19	M232	15281484-5036067	15 28 14.84	-50 36 6.70	14.27	13.62	13.49		
M151	15275290-5043446	15 27 52.90	-50 43 44.60	14.16	13.4	13.29	M238	15283233-5039196	15 28 32.33	-50 39 19.60	14.1	13.53	13.44		
M152	15281401-5043171	15 28 14.02	-50 43 17.10	14.1	13.47	13.3	M240	15275299-5035315	15 27 52.99	-50 35 31.50	13.67	12.96	12.9		
M160	15275246-5037111	15 27 52.46	-50 37 11.10	14.09	13.49	13.39	M250	15275112-5035252	15 27 51.13	-50 35 25.20	13.84	13.21	13.14		
M193	15281966-5037402	15 28 19.67	-50 37 40.20	13.73	13.15	12.95	M253	15273924-5044470	15 27 39.24	-50 44 47.00	14.01	13.41	13.33		
M199	15273464-5039364	15 27 34.64	-50 39 36.40	13.96	13.36	13.25	M256	15283486-5039461	15 28 34.86	-50 39 46.10	14.11	13.4	13.26		
M204	15282525-5038375	15 28 25.25	-50 38 37.50	14.13	13.46	13.42	M264	15273567-5044373	15 27 35.67	-50 44 37.30	13.72	12.97	12.83		
M228	15274983-5045114	15 27 49.82	-50 45 11.40	14.19	13.5	13.41	M276	15275546-5034378	15 27 55.47	-50 34 37.80	14.39	13.64	13.65		
M230	15280455-5035385	15 28 4.55	-50 35 38.50	14.32	13.54	13.48	M285	15272593-5037513	15 27 25.93	-50 37 51.30	13.99	13.33	13.22		
M235	15281153-5045171	15 28 11.53	-50 45 17.10	13.86	13.22	13.04	M291	15283744-5043066	15 28 37.44	-50 43 6.60	13.83	13.2	13.14		
M244	15273214-5043148	15 27 32.14	-50 43 14.80	14.17	13.51	13.45	M295	15283057-5036006	15 28 30.57	-50 36 0.60	13.68	12.99	12.87		
M248	15283429-5040506	15 28 34.29	-50 40 50.60	14.14	13.45	13.29	M297	15274935-5046549	15 27 49.35	-50 46 54.90	13.84	13.19	13.01		
M252	15282894-5037295	15 28 28.94	-50 37 29.50	13.86	13.21	13.03	M303	15275659-5033401	15 27 56.58	-50 33 40.10	13.78	13.18	13.05		
M255	15283059-5043177	15 28 30.59	-50 43 17.70	14.36	13.64	13.62	M304	15281049-5047189	15 28 10.50	-50 47 18.90	13.99	13.25	13.11		
M258	15272726-5039069	15 27 27.26	-50 39 6.90	13.89	13.29	13.12	M320	15275396-5033273	15 27 53.96	-50 33 27.30	14.4	13.72	13.53		
M260	15282799-5037075	15 28 27.99	-50 37 7.50	14.11	13.47	13.4	M321	15284225-5043270	15 28 42.25	-50 43 27.00	14.17	13.54	13.48		
M263	15274309-5045256	15 27 43.09	-50 45 25.60	13.98	13.3	13.16	M322	15273763-5034221	15 27 37.63	-50 34 22.10	13.96	13.28	13.1		
M267	15275749-5034515	15 27 57.49	-50 34 51.50	13.99	13.36	13.23	M323	15271949-5037310	15 27 19.49	-50 37 31.10	13.89	13.18	13.07		
M270	15272780-5043096	15 27 27.80	-50 43 9.60	14.11	13.44	13.34	M327	15284176-5043473	15 28 41.76	-50 43 47.30	14.36	13.76	13.7		
M273	15283082-5037019	15 28 30.82	-50 37 1.90	14.04	13.44	13.29	M328	15282266-5046563	15 28 22.66	-50 46 56.30	14.22	13.5	13.38		
M284	15272199-5040260	15 27 21.99	-50 40 26.00	14.01	13.36	13.28	M330	15284533-5038336	15 28 45.34	-50 38 33.60	13.87	13.23	13.02		
M299	15284050-5042394	15 28 40.50	-50 42 39.40	14.12	13.45	13.34	M333	15284603-5038547	15 28 46.03	-50 38 54.70	14.16	13.51	13.38		
M300	15272430-5037136	15 27 24.30	-50 37 13.60	13.79	13.22	13.11	M335	15275184-5033162	15 27 51.84	-50 33 16.20	13.89	13.28	13.19		
M305	15284385-5039233	15 28 43.85	-50 39 23.30	13.96	13.24	13.09	M341	15271362-5039331	15 27 13.62	-50 39 33.10	14.22	13.57	13.49		
M308	15271847-5042403	15 27 18.48	-50 42 40.30	13.98	13.33	13.18	M349	15280909-5032594	15 28 9.09	-50 32 59.40	14.36	13.78	13.54		
M319	15282577-5046327	15 28 25.77	-50 46 32.70	14.11	13.42	13.3	M356	15271166-5041490	15 27 11.66	-50 41 49.10	13.73	12.98	12.85		
M326	15284338-5043099	15 28 43.38	-50 43 9.90	13.7	13.13	13.05	M360	15274912-5048166	15 27 49.12	-50 48 16.60	14.25	13.56	13.4		
M339	15281136-5033166	15 28 11.36	-50 33 16.60	13.97	13.38	13.23	M362	15284867-5038134	15 28 48.67	-50 38 13.40	14.22	13.54	13.38		
M342	15273444-5046503	15 27 34.44	-50 46 50.30	14.4	13.74	13.59	M383	15271519-5037093	15 27 15.19	-50 37 9.30	13.82	13.15	13.02		
M351	15271434-5038173	15 27 14.34	-50 38 17.30	13.89	13.26	13.05									
M354	15271189-5040378	15 27 11.89	-50 40 37.80	13.7	13.02	12.9									
M357	15284217-5036124	15 28 42.17	-50 36 12.40	14.07	13.41	13.33									

Columns two and nine are the 2MASS identifications for target RGB stars. Columns three, four, ten and eleven give the R.A. and Dec. of the GIRAFFE fibre used to observe the star. The final columns are the 2MASS  $JHK_S$  magnitudes.

Instead we synthesized a template spectrum with  $T_{\text{eff}}=6000$  K,  $\log g=4.0$ , and  $[\text{Fe}/\text{H}]=-0.25$ .

The radial velocities of the TO targets may be expected to be more uncertain than the other velocities because the synthetic template contains errors and line omissions due to our imperfect knowledge of the atomic parameters of all the lines in this region of the optical spectrum. Also, the synthetic template does not have exactly the same wavelength scale. However, Griffin et al. (2000) indicate that radial velocity errors are greatest when the line broadening in the template spectrum does not match the target spectrum. Griffin et al. (2000) find that radial velocity errors introduced by target-template mismatches are  $\pm 0.5$  km s<sup>-1</sup> or less.

The procedure to measure the mean radial velocity for a given star differs depending on the type of star. For the HB and RGB candidates stars we determine the radial velocities in two ways – first by cross-correlating a template spectrum with the final, combined spectrum for the stars and secondly by measuring the radial velocity for each of the individual 20 OBs, from which we can calculate a mean and standard deviation. The two meth-

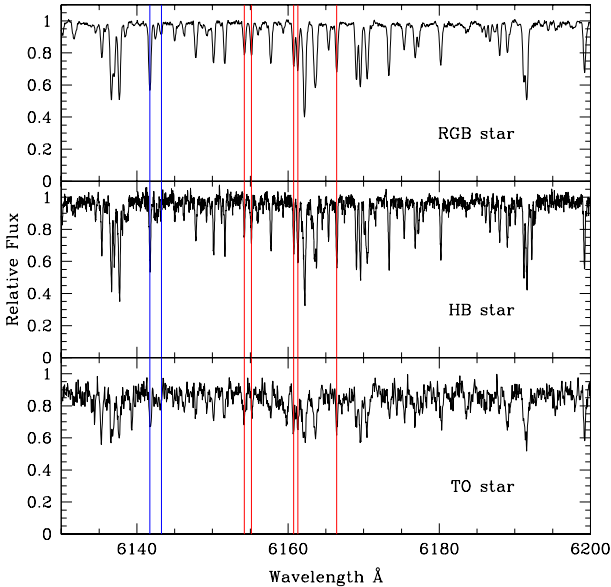
ods give extremely similar final radial velocities but the latter method indicates a larger, and we would argue more realistic,  $\sigma$  (error). Figure 4 shows a comparison between the resulting error-estimates for the two methods. We note that deriving radial velocities from individual spectra has the advantage of highlighting stars with variable radial velocities (see section 4.1). We adopt the average over individually measured OBs as our final radial velocity value.

Table 1 gives the final radial velocities and error estimates for the HB/RGB-UVES stars. Table 5 lists our final radial velocities and error estimates for the RGB-GIRAFFE stars. Some RGB-GIRAFFE stars were not observed across all 20 OBs. For those stars observed in every OB, not all stars have 20 spectra for which FXCOR would give satisfactory results (e.g., strong cosmic ray features in a single OB that averaged out in the combined spectrum). A  $3\sigma$  clipping was applied in the final calculation of the radial velocities for the RGB and HB stars. For eight RGB-GIRAFFE stars (M098, M160, M211, M232, M248, M321, M333, and M357) one measurement was rejected thanks to this clipping scheme (see also Table 5). In most cases, once

**Table 4.** Observing dates, exposure times, average seeing, airmass, and helio-centric corrections for all observations. Note that the OBs are listed in the order they were executed.

Observing Block	Date	UT	JD	Exp-time [s]	Average seeing during obs. ["]	Airmass	Helio-centric correction [km s <sup>-1</sup> ]
281555	2007 05 12	02:48:23.543	2454232.62184	3600	1.16±0.45	1.22	5.74
281556	2007 05 12	05:43:13.406	2454232.74325	3600	1.27±0.60	1.13	5.49
281557	2007 05 12	06:50:11.231	2454232.78976	3600	1.23±0.54	1.22	5.39
281558	2007 05 12	07:52:11.744	2454232.83282	3600	1.24±0.58	1.37	5.32
281559	2007 05 13	01:32:58.649	2454233.56949	3600	0.92±0.01	1.42	5.40
281560	2007 05 15	00:05:47.728	2454235.50897	3600	0.59±0.01	1.88	4.62
281561	2007 05 15	01:11:22.661	2454235.55452	3600	0.42±0.01	1.48	4.56
281562	2007 05 17	02:03:43.510	2454237.59090	3600	0.86±0.01	1.28	3.64
281563	2007 05 20	00:49:43.705	2454240.53954	3600	1.15±0.44	1.49	2.42
281564	2007 05 22	02:53:50.236	2454242.62574	3600	1.47±0.87	1.16	1.40
281565	2007 05 22	03:58:41.221	2454242.67077	3600	1.54±0.93	1.11	1.30
281566	2007 06 17	05:09:48.056	2454268.71979	3600	1.24±0.57	1.31	-9.77
281567	2007 06 22	00:38:31.127	2454273.53123	3600	2.13±1.62	1.17	-11.36
281568	2007 06 22	01:45:56.216	2454273.57805	3600	1.58±1.00	1.12	-11.45
281569	2007 06 22	02:52:30.930	2454273.62428	3600	1.26±0.59	1.13	-11.55
281570	2007 06 22	04:04:06.944	2454273.67400	3600	1.24±0.56	1.21	-11.64
281574	2007 07 19	00:37:24.431	2454300.52901	3600	0.72±0.01	1.11	-20.20
281573	2007 07 20	00:40:29.476	2454301.53108	3600	1.36±0.74	1.12	-20.46
281572	2007 07 20	01:42:01.361	2454301.57381	3600	0.89±0.01	1.16	-20.54
281571	2007 07 22	00:48:44.083	2454303.53667	3600	1.24±0.56	1.12	-20.97

Column one lists the name of the observing block, column two the date the observations were taken, columns three and four give the starting time of the observation (in UT) and the Julian date, column five lists the exposure time, column six the average seeing during the observation including a  $\sigma$  and column seven the airmass at which the observations were carried out. The last column lists the helio-centric corrections derived in this work and applied when combining spectra from each of the 20 OBs into one single spectrum.



**Fig. 3.** A section of three of our target spectra: M151, NGC 5927-05, and T021. The spectra are arranged in order of increasing S/N. Two blue lines (to the left) indicate the location of the Ba II and Zr I lines at 614.17 nm and 614.31 nm, respectively. The five red lines indicate the position of the Si I line at 615.51 nm, the Na I lines at 615.42 nm and 616.07 nm, and the Ca I lines at 616.13 nm, and 616.64 nm, respectively.

the deviating individual spectrum was removed the remaining measurements fell within  $1\sigma$ .

For the TO stars the individual spectra are too noisy to yield satisfactory results and we thus only measured their radial velocities using the final, combined spectra. The results are listed in Table 2. The error reported by IRAF is typically between 1.0 and 1.5 km s<sup>-1</sup> for the combined TO spectra and between 0.20 and 0.5 km s<sup>-1</sup> for the RGB-GIRAFFE and HB/RGB-UVES stars. Our tests with the RGB-GIRAFFE stars indicate that those errors do not reflect the true uncertainty in the radial velocity measurement over several OBs for stars observed with the Medusa fibres (see Table 5). However, the IRAF error is consistent with the  $\sigma(\text{OB})$  for the UVES stars, where the higher resolving power affords us greater accuracy (see Table 1). An additional source of error is the decreasing S/N. Even for the combined TO spectra the S/N is low, perhaps resulting in a slightly worse determination of the radial velocity. Fortunately, the turn-off velocity distribution is very clean: the member and non-member stars are very distinctly separated in radial velocity (see Table 2 and Fig. 7). Therefore the precise value of the uncertainty in radial velocity makes no practical difference for the TO candidates.

#### 4.1. Comments on individual stars

**M227** This star was selected as a potential RGB star. Instead of a relatively clean RGB spectrum we have a very rich spectrum full of molecular band-heads. Figure 5 shows a section of the spectrum of M227 and the cluster member star M151 for comparison. It was not possible to determine a radial velocity for M227 with either of our templates. Given the position of M227 in the 2MASS CMD, it is unlikely that it is an M giant (or that it is behind the same interstellar extinction as NGC 5927). M227 is most probably an intrinsically red foreground dwarf star.

**Table 5.** Radial velocities for RGB-GIRAFFE targets. Both member stars in NGC 5927 (left column) as well as non-members (right panel) are listed-

Star	Cluster members			Star	Cluster non-members		
	R.V. [km s <sup>-1</sup> ]	$\sigma$ [km s <sup>-1</sup> ]	Comments		R.V. [km s <sup>-1</sup> ]	$\sigma$ [km s <sup>-1</sup> ]	Comments
M003	-94.65	0.66		M130	-4.198	3.98	See Sect 4.1
M012	-98.08	0.64		M138	+11.24	0.89	
M061	-101.4	0.88		M171	-29.01	0.93	
M098	-104.9	0.99	1 rej	M211	-82.82	0.79	
M111	-109.0	1.39		M213	-51.61	0.72	
M115	-101.8	0.74		M222	-27.92	1.08	
M120	-115.6	0.72		M227			See Sect 4.1
M126	-99.52	1.32	5 spectra	M232	-30.0	0.94	13 spectra
M151	-95.39	0.79		M238	+70.63	3.25	See Sect 4.1
M152	-109.9	0.76	18 spectra	M240	-142.4	2.91	See Sect 4.1
M160	-109.5	0.67	1 rej	M250	-54.72	0.59	
M193	-107.8	0.19		M253	-72.37	0.72	19 spectra
M199	-102.8	0.47		M256	-69.14	0.73	19 spectra
M204	-110.0	0.80	19 spectra	M264	-76.72	0.58	
M228	-108.2	1.31		M276	-85.43	1.09	
M230	-106.2	0.79		M285	-42.35	1.13	
M235	-103.4	0.95		M291	+61.45	1.05	
M244	-105.6	3.00	See Sect 4.1	M295	-74.93	0.57	
M248	-111.5	0.60	19 spectra	M297	-56.41	0.92	
M252	-98.51	0.76	18 spectra	M303	-47.3	0.77	
M255	-104.8	1.11		M304	+8.44	0.69	
M258	-99.11	0.63		M320	-17.7	0.55	
M260	-99.67	0.75		M321	-138.0	0.76	1 rej
M263	-100.9	0.84		M322	-49.1	2.14	18 spectra
M267	-101.8	1.04		M323	-130.6	0.66	19 spectra
M270	-108.6	0.84		M327	-54.9	0.66	19 spectra
M273	-105.6	0.73		M328	-45.3	1.46	17 spectra
M284	-106.5	1.24		M330	-27.1	0.59	19 spectra
M299	-105.8	1.01		M333	+20.3	0.66	1 rej
M300	-106.1	1.18	19 spectra	M335	-65.1	0.82	
M305	-97.61	0.56		M341	-36.5	1.96	See Sect 4.1
M308	-110.3	0.71	19 spectra	M349	-53.0	9.11	See Sect 4.1
M319	-106.6	0.84		M356	-20.4	0.69	
M326	-107.1	1.31		M360	-141.6	0.28	
M339	-101.8	0.89	19 spectra	M362	-8.8	0.42	
M342	-102.9	0.70		M383	-61.0	0.62	
M351	-106.4	0.74					
M354	-93.3	0.92					
M357	-101.5	0.87	1 rej				

The first and fifth columns list the ID for the star. The second and sixth columns give our final radial velocity for the star and the third and seventh column lists the sigma of the 20 individual measurements that the radial velocity is based on. For some stars one spectrum were rejected from the final averaged spectrum. For some stars less than 20 spectra were available (e.g., due to faulty fibres or miss-placements). The number of available spectra is noted in case it less than 20. Stars discussed individually in Sect 4.1 are also indicated.

**M238** This star was selected as a potential RGB star. We note, based on visual inspection of the spectrum, that this star most likely is quite a bit more metal-poor than the majority of the stars observed. In Fig. 5 we show a section of the spectrum of M238 and the cluster member M151 for comparison. M238 is not a radial velocity member of NGC 5927.

**M130, M238, M240, M244, and M349** These five stars were selected as potential RGB stars. They all show temporal variability in their radial velocities, as illustrated in Fig. 6. Our observations are clumped in time. For M130, M238, and M244 there is not much variation within each group of observations carried out close in time, but the variability shows up on longer timescales. M349 and M240 have the potential for variability on a much shorter time scale. The difference between maximum and mini-

um velocity is around 10 km s<sup>-1</sup> for all stars but M349, where the difference is as large as 20 km s<sup>-1</sup>. All five stars show a radial velocity variation at least 2.5 times larger than the average standard deviation across all 20 OBs for all our RGB-GIRAFFE targets ( $\sigma = 1.2\text{km s}^{-1}$ ).

Since the fibre configuration was not constant across all 20 OBs we have investigated the possibility that stars were misidentified, either through improper fibre positioning or faulty fibre-star matching. In all cases fibre coordinates were well matched to the correct stellar coordinates. Furthermore, fibre configuration changes do not correlate with the observed radial velocity variations. Radial velocity variations as large as these typically indicate stellar companions. There is no indication of a secondary spectrum in any of these cases. We note that of these five potential binary systems only M244 is a radial velocity member of NGC 5927 (see Table 5).

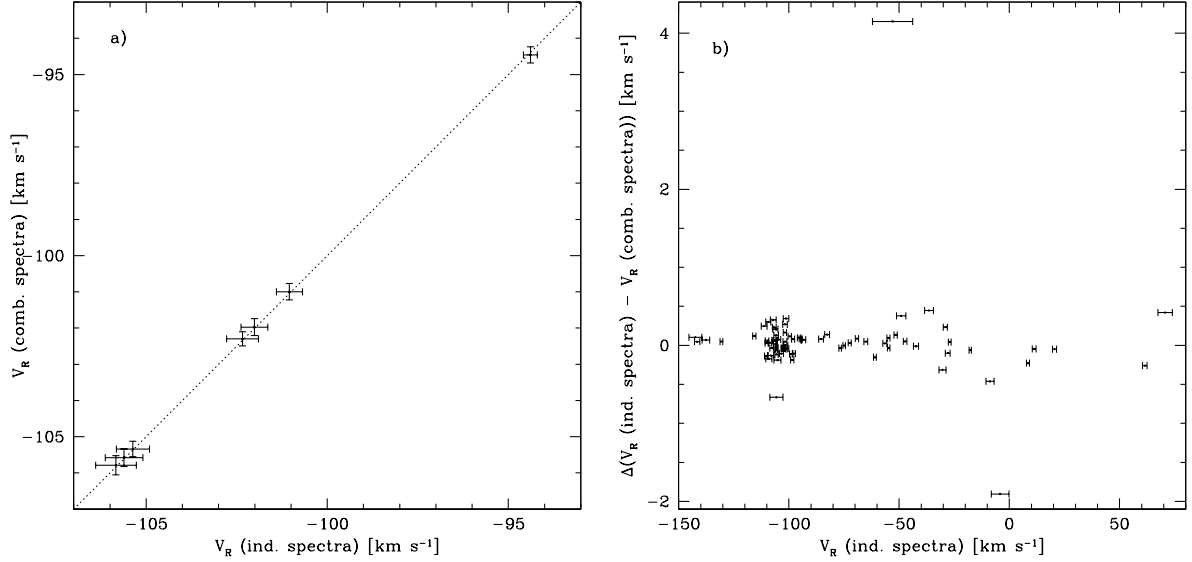


**Fig. 4.** **a)** Comparison of radial velocities for the HB/RGB-UVES stars derived from the combined spectrum (y-axis) and from the up to twenty individual spectra separately and then averaged (x-axis). Errors bars refer for the y-axis to errors as estimated by IRAF (see text) and for the x-axis to the  $\sigma$  around the mean. The dotted line shows the one-to-one relation. **b)** Shows the difference between the radial velocities for RGB-FLAMES stars derived from the up to twenty individual spectra separately and averaged and the radial velocities derived from the combined spectra as a function of the radial velocities derived the individual spectra and averaged. We only show the errors bars for these values as they are by far the largest. N.B. the radial velocities based on the individual spectra are shown before the culling leading to the final radial velocities shown in Table 5.

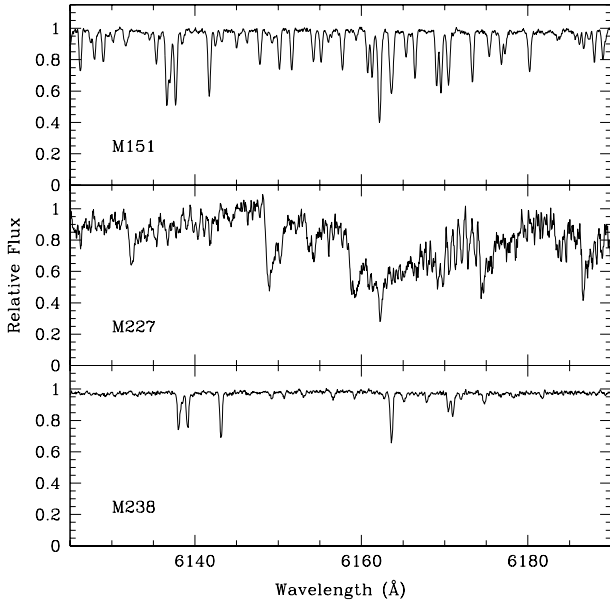


**Fig. 5.** Sections of spectra for three RGB-GIRAFFE stars. The upper panel shows M151, which we find to be a radial velocity member of NGC 5927. The middle panel shows a portion of the spectrum for M227, which is a cool foreground dwarf star. The bottom panel shows the spectrum of an RGB star that is significantly more metal-poor than the majority of the stars in the cluster.

M341 and M322 These stars were selected as potential RGB stars. They have a very large  $\sigma$  for the radial velocities when all OBs are considered, but radial velocity measurements from individual OBs fall within  $3\sigma$  of the final value. We have not

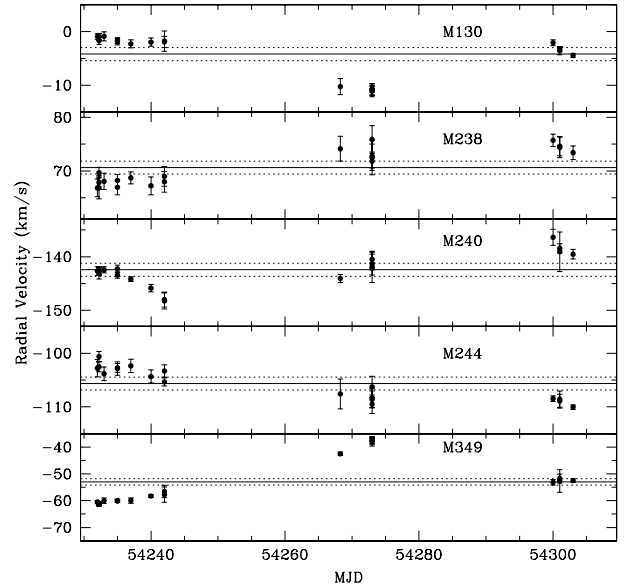


**Fig. 6.** The measured radial velocity is shown as a function of the modified Julian date (MJD) for five stars that display unusually large temporal variations in their measured velocities. The vertical extent of all five panels is  $\pm 20$  km s<sup>-1</sup> from the average radial velocity of the star (shown with a solid line). The dotted line indicates  $\pm 1.2$  km s<sup>-1</sup>, which is the average radial velocity  $\sigma$  for the entire RGB-GIRAFFE sample. Of these five stars only M244 has an average radial velocity consistent with membership of NGC 5927.

been able to identify anything that might explain the large  $\sigma$ . Neither star is a radial velocity member.

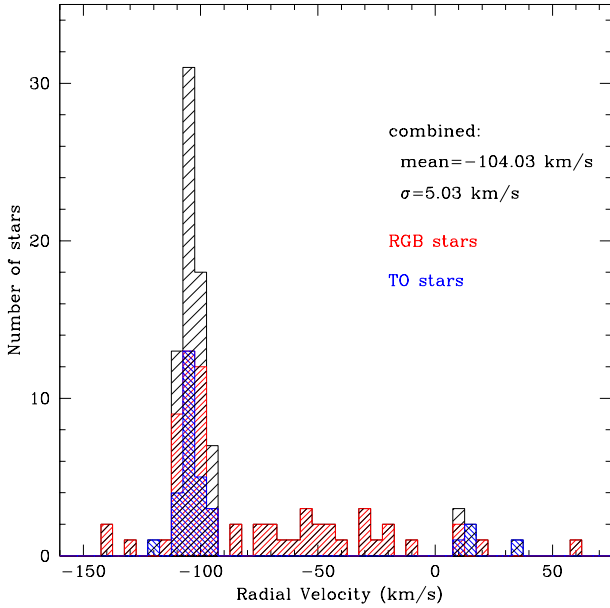


**Fig. 7.** The distribution of measured heliocentric radial velocities for our target stars. Radial velocity variables are excluded. The black histogram is the combined sample. The red and blue histograms are the RGB-GIRAFFE and TO samples, respectively.

## 5. Cluster membership and the radial velocity of NGC 5927

Figure 7 shows our derived velocity histograms for the heliocentric radial velocities of the targeted stars. Stars showing radial velocity variability have been excluded (see section 4.1). It is clear that the RGB-GIRAFFE sample in the outer part of the cluster contributes most of the background/foreground contamination. The majority of the TO candidates are members of the cluster.

The relatively large number of RGB-GIRAFFE candidates and the relatively high fraction of non-members make an iterative rejection necessary. First, we considered only stars with  $-150 \text{ km s}^{-1} < v_r < -70 \text{ km s}^{-1}$ , since it is clear that the systemic velocity for the cluster must be in this range. Next, we calculated the mean and standard deviation ( $\sigma$ ) of the radial velocities for all target stars with measured radial velocities in that range. Then, we excluded stars more than  $3\sigma$  from the initial mean value. Finally, we re-calculated the mean velocity from the culled sample. We iterated in this way until we could exclude no more stars with a  $3\sigma$ -clipping. We need 4 further iterations to reach the final value. In this way we derive a mean velocity for NGC 5927 of  $-104.03 \text{ km s}^{-1}$  with  $\sigma = 5.03 \text{ km s}^{-1}$ .

This resulted in the 72 stars (RGB-UVES, RGB-GIRAFFE, and TO) that satisfy the membership criteria. All of our RGB-UVES targets are radial velocity members and 26 of our 30 TO candidates are radial velocity members. Our RGB-GIRAFFE candidate success rate is much lower: only 39 of our 75 target stars are  $3\sigma$  members of NGC 5927, i.e. a 50%.

Since NGC 5927 lies in the plane of the Milky Way foreground contamination in the cluster outskirts is quite likely. We have much greater success in the inner  $5''$ . Radial velocity studies with small numbers of stars or limited to the outer regions of the cluster thus may suffer from a large number of non-member stars. If we had been limited to target selection from ground-based photometry (i.e. not accessing the crowded core) and/or had had fewer targets overall, it is quite likely our systemic ra-

dial velocity would have skewed to lower values, where the bulk of the foreground contamination lies.

There are several determinations for the radial velocity for NGC 5927 in the literature (see Table 6). One third of the available estimates are based on integrated light rather than single stars.

The spread in radial velocities within a single study can be quite large. For example, although Kinman (1959) reports an average radial velocity of  $-96 \text{ km s}^{-1}$  (based on 6 stars) individual measurements range from  $-204 \text{ km s}^{-1}$  to  $+3 \text{ km s}^{-1}$ . Two stars fall at  $-118 \text{ km s}^{-1}$  and two close to  $-70 \text{ km s}^{-1}$ . We suspect that their sample is heavily contaminated with foreground and background stars. Webbink (1981) is a compilation based primarily on Kinman (1959) but with the addition of a single Mira variable from Andrews et al. (1974). Webbink (1981) reports a weighted average of radial velocity values but contamination can not be excluded.

Cohen (1983) reports radial velocities from individual stars. Her mean velocity is low compared to almost all other determinations. However, Cohen (1983) does report instrument difficulties that limited the internal measurement accuracy to  $15 \text{ km s}^{-1}$ . The scatter around the mean value is large,  $\sigma = 15 \text{ km s}^{-1}$ .

We note that the value from Carrera et al. (2007) differs the most (when considering results based on individual stars). A likely explanation is that these observations were taken with FORS2 on the VLT, i.e., a low resolution ( $R \sim 5000$ ), multi-slit spectrograph where misalignments between stars and slits hampered the determination of the radial velocities. This offset can produce differences in radial velocities of about  $15 \text{ km s}^{-1}$  (the  $\sigma$  quoted in Table 6 is the scatter around the mean value). A realistic error in the radial velocity would be  $10 - 15 \text{ km s}^{-1}$  (Carrera, *priv. com.*). Carrera et al. (2007) were primarily concerned with measuring the strength of the Ca II triplet lines and hence this was not problematic for their science case.

The difference can likely be traced to that the observations in Carrera et al. (2007) were obtained in MXU mode (multi-slit) and not long-slit. Since the masks are created prior to the actual observations it can be difficult to ensure that all stars are properly placed on the slits resulting in decreased accuracy for the radial velocities and can account for the observed discrepancies (Carrera, *priv. com.*). This can become a significant problem, e.g., if the seeing is smaller than the actual slit width. That this is a potential problem for observations with the FORS instruments has been previously reported in the literature (e.g., Irwin & Tolstoy 2002). We note that for NGC 6532 Feltzing et al. (2009) derive a radial velocity  $\sim 20 \text{ km s}^{-1}$  larger than the value from Carrera et al. (2007). Again, likely resulting from the same cause.

Pancino et al. (2010) obtained velocities for a large number of stars in NGC 5927. Our value agrees well with theirs within the error-bars. Finally, we note that of all the single-star radial velocity measurements in the literature, only Suntzeff et al. (1993) reports having observed stars that are not radial velocity members and we have excluded those from the average in Table 6. Our average radial velocity agrees very well their value.

## 6. Summary

We have obtained spectra of 105 stars in the direction of the metal-rich globular cluster NGC 5927 using the UVES and GIRAFFE fibres in the FLAMES spectrograph. Based on the measured radial velocities we identified the following members of NGC 5927:

**Table 6.** Radial velocities for NGC 5927 from the literature.

Radial velocity [km s <sup>-1</sup> ]	$\sigma$ [km s <sup>-1</sup> ]	No. of objects	Type of obs.	Reference
-96	$\pm 28$		Integrated light	Kinman (1959)
-78	$\epsilon=12$	7	Compilation	Webbink (1981) †
-74	$\pm 15$	6	Individual stars	Cohen (1983)
-93	$\pm 14$		Integrated light	Zinn & West (1984)
-106	$\pm 7$		Integrated light	Hesser et al. (1986)
-113			Integrated light	Armandroff & Zinn (1988) (no error)
-106.6	$\pm 5.2$	8	Individual stars	Suntzeff et al. (1993) ††
-118.6	$\pm 8.8$	5	Individual stars	Da Costa & Armandroff (1995)
-123.8	$\pm 8.8$	19	Individual stars	Rutledge et al. (1997b)
-84	$\pm 5$	20	Individual stars	Carrera et al. (2007)
-110.3	$\pm 21.5$	43	Individual stars	Pancino et al. (2010)
-104.03	$\pm 5.03$	70	Individual stars	This work

The first column lists the heliocentric radial velocity. The second column lists the number of stars used in the derivation of the mean velocity of the cluster. For four studies integrated light has been used instead, as indicated. Column three lists the reference for the measurement. Any additional comments are given in column four.

† For a description of the calculation of the total error, including stellar variability, see Webbink (1981).

†† Average excludes star M468 and star A.

- 7 HB and RGB stars with high-resolution spectra
- 39 HB and RGB stars with medium-resolution spectra
- 26 TO stars with medium-resolution spectra

We also found:

- one foreground cool dwarf star,
- one likely very metal-poor, giant or subgiant star,
- five radial velocity variables with no companion star visible in the spectrum of the primary. One of these variables is a radial velocity member of NGC 5927.

Our final radial velocity,  $v_r = -104.03 \pm 5.03$  km s<sup>-1</sup>, agrees well with the majority of most recently published values, but is based on a much larger sample of high-quality spectra.

*Acknowledgements.* We thank the referee, R. Carrera, for a careful read of the manuscript and valuable suggestions that increased the readability of the paper. We would in particular like to thank him for the useful information on the FORS2 observations (Carrera et al. 2007) which gives a likely explanation to the discrepancy between our and their values for the radial velocities.

We would like to thank Rachel A. Johnson for her work in the identification of target stars for this observing program. We would also like to thank Thomas Brown for providing the ACS data. JS acknowledges the support of an Incoming International Marie Curie Fellowship. SF is a Royal Swedish Academy of Sciences Research Fellows supported by a grant from the Knut and Alice Wallenberg Foundation. SF acknowledges support from grant number 2008-4095 from the Swedish Research Council. This work has made use of the NED, SIMBAD, and VALD databases. This publication makes use of data products from the Two Micron All Sky Survey, which is a joint project of the University of Massachusetts and the Infrared Processing and Analysis Center/California Institute of Technology, funded by the National Aeronautics and Space Administration and the National Science Foundation.

## References

Andrews, P. J., Feast, M. W., Lloyd Evans, T., Thackeray, A. D., & Menzies, J. W. 1974, *The Observatory*, 94, 133  
 Armandroff, T. E. 1989, *AJ*, 97, 375  
 Armandroff, T. E. & Zinn, R. 1988, *AJ*, 96, 92  
 Bedin, L. R., Cassisi, S., Castelli, F., et al. 2005, *MNRAS*, 357, 1038  
 Bica, E., Bonatto, C., Barbuy, B., & Ortolani, S. 2006, *A&A*, 450, 105  
 Brown, T. M., Ferguson, H. C., Smith, E., et al. 2005, *AJ*, 130, 1693  
 Brown, T. M., Ferguson, H. C., Smith, E., et al. 2004, *ApJ*, 613, L125  
 Carrera, R., Gallart, C., Pancino, E., & Zinn, R. 2007, *AJ*, 134, 1298  
 Casetti-Dinescu, D. I., Girard, T. M., Herrera, D., et al. 2007, *AJ*, 134, 195  
 Casetti-Dinescu, D. I., Girard, T. M., Korchagin, V. I., van Altena, W. F., & López, C. E. 2010, *AJ*, 140, 1282

Cohen, J. G. 1983, *ApJ*, 270, 654  
 Da Costa, G. S. & Armandroff, T. E. 1995, *AJ*, 109, 2533  
 Dinescu, D. I., Girard, T. M., & van Altena, W. F. 1999a, *AJ*, 117, 1792  
 Dinescu, D. I., Girard, T. M., van Altena, W. F., & López, C. E. 2003, *AJ*, 125, 1373  
 Dinescu, D. I., van Altena, W. F., Girard, T. M., & López, C. E. 1999b, *AJ*, 117, 277  
 Feltzing, S., Primas, F., & Johnson, R. A. 2009, *A&A*, 493, 913  
 Griffin, R. E. M., David, M., & Verschueren, W. 2000, *A&AS*, 147, 299  
 Harris, W. E. 1996, *AJ*, 112, 1487  
 Hesser, J. E., Shawl, S. J., & Meyer, J. E. 1986, *PASP*, 98, 403  
 Irwin, M. & Tolstoy, E. 2002, *MNRAS*, 336, 643  
 Kinman, T. D. 1959, *MNRAS*, 119, 157  
 Kraft, R. P. & Ivans, I. I. 2003, *PASP*, 115, 143  
 Law, D. R. & Majewski, S. R. 2010, *ApJ*, 718, 1128  
 Pancino, E., Rejkuba, M., Zoccali, M., & Carrera, R. 2010, *A&A*, 524, A44  
 Pasquini, L., Avila, G., Blecha, A., et al. 2002, *The Messenger*, 110, 1  
 Rutledge, G. A., Hesser, J. E., & Stetson, P. B. 1997a, *PASP*, 109, 907  
 Rutledge, G. A., Hesser, J. E., Stetson, P. B., et al. 1997b, *PASP*, 109, 883  
 Santos, Jr., J. F. C. & Piatti, A. E. 2004, *A&A*, 428, 79  
 Skrutskie, M. F., Cutri, R. M., Stiening, R., et al. 2006, *AJ*, 131, 1163  
 Suntzeff, N. B., Mateo, M., Terndrup, D. M., et al. 1993, *ApJ*, 418, 208  
 Thomas, D., Maraston, C., & Bender, R. 2003, *MNRAS*, 339, 897  
 Webbink, R. F. 1981, *ApJS*, 45, 259  
 Zinn, R. 1985, *ApJ*, 293, 424  
 Zinn, R. & West, M. J. 1984, *ApJS*, 55, 45